Journal of Thermal Science Vol.32, No.6 (2023) 2256−2272

https://doi.org/10.1007/s11630-023-1720-3 **Article ID: 1003-2169(2023)06-2256-17**

Optimization of Fuel In-Situ Reduction (FISR) Denitrification Technology for Cement Kiln using CFD Method

SHI Chaoting[1,2], CAI Jun[1,2,3*], REN Qiangqiang[1,2,3], WU Huixing[1,2]

1. Institute of Engineering Thermophysics, Chinese Academy of Sciences, Beijing 100190, China
2. University of Chinese Academy of Sciences, Beijing 100049, China
3. Dalian National Laboratory for Clean Energy, Dalian 116023, China

Abstract: Nitrogen oxides (NO_x) from cement industry have drawn more and more attention and the existing denitrification technologies can hardly meet the increasingly stringent emission requirements in China. In our previous work, fuel in-situ reduction (FISR) method was proposed to cut cement NO_x emission. With the pilot-scale precalciner in the previous experiment as objection, optimization of FISR method was conducted using CFD method. The results demonstrated that NO_x emission decreased by 69.86% after adopting FISR method. The effects of initial concentrations of NO and O_2 in kiln gas, feeding location of the first-stage tertiary (tertiary air-I) and cement raw meal (CRM) were further investigated. With increasing initial NO concentration, NO_x emission increased linearly, while the reduction rate of NO in kiln gas maintained above 80%. When O_2 content in kiln gas is more than 4%, oxygen would more significantly promote the formation of NO_x and inhibit the reduction of NO. The dimensionless locations of tertiary air-I and CRM were introduced. The simulation results showed that the optimal dimensionless locations are 0.6 and 1.6 for tertiary air-I and CRM, respectively. The outputs achieved in this study will provide a strong support for the practical application of FISR method in cement industry.

Keywords: cement industry, precalciner, pretreated fuel, NO_x emission, denitrification

1. Introduction

China is the most important cement producer and consumer in the world, and the cement production has reached 2.38 billion tons in 2020 [1]. However, cement production is a crucial source of nitrogen oxides (NO_x), which is why the cement industry has become the third largest emission source since thermal power generation and transportation [2, 3]. NO_x have been considered to be the precursors of photochemical fog and acid rain, imposing a significant threat to human life [4]. Achieving ultra-low NO_x emission has become an essential objective of cleaner production in cement industry [5].

The dry-process cement clinker production technology is applied extensively, in which both precalciner and rotary kiln are responsible for producing NO_x. Cement raw meal (CRM) is heated to 750°C–800°C by exhaust gas (defined as the flue gas from the precalciner) and then sent to the precalciner for decomposing. About 60% of the total pulverized coal (PC) is supplied to the precalciner, in which the temperature is within 870°C–1050°C. Then, the decomposed CRM enters the rotary

Received: Apr 19, 2021
AE: YANG Bin

Corresponding author: CAI Jun E-mail: caijun@iet.cn

kiln, where the clinkering reactions occur with temperature above 1450°C. Without any de-NO_x technologies, the original NO_x concentrations in kiln gas (defined as the flue gas from the rotary kiln) and in the exhaust gas could be as high as 0.7×10^{-3}–1.2×10^{-3} (in volume) [6] and 4.0×10^{-4}–6.0×10^{-4} (in volume) [7], respectively.

The existing denitrification methods in cement industry can be divided into three categories: pre-combustion, combustion and post-combustion [8]. For the pre-combustion method, adding minerals into CRM can inhibit thermal NO_x by 5%–10% because of lowering the sinter temperature. However, this kind of method may decrease the quality of clinker, and the ability of nitrogen denitrification in cement production is limited. The second category methods reduce NO_x emission by reasonably organizing combustion in the rotary kiln and the precalciner. Low NO_x burner is extensively used in the rotary kiln and can realize about 10%–15% denitrification efficiency [9]. Whereas, in view of the increasing enthusiasm of using inferior coal in China, it is necessary to further develop low NO_x burners to improve its adaptability to low-grade fuel. Traditional staged combustion (TSC) technology has a good NO_x reduction effect under lab-scale conditions [10–12] and has been widely used in the precalciner. However, only 15%–25% of the fuel-NO_x can be hindered when TSC technology is used alone in actual cement production. The third category methods mainly refer to selective non-catalytic reduction (SNCR) technology. As opposed to SNCR used in power station boilers, NO_x reduction efficiency of SNCR in cement industry is unstable, varying from 15% to 80% [13] because of the complex atmosphere in the precalciner, where both combustion and CRM decomposition are interwoven with NO_x reduction. Besides, the escapement of ammonia results in a secondary pollution.

According to the actual measurement data during cement production, the NO_x emission concentration can reach 300–400 mg/m^3 with combination of the low nitrogen burner, TSC and SNCR technologies, which can meet the current emission standard of air pollutants for cement industry in China. However, with the increasing awareness of environmental protection, some local provinces in China have issued more stringent NO_x emission standard, such as Jiangsu, Henan, Hebei, Zhejiang and Ningxia provinces. Although selective catalytic reduction (SCR) technology has become the mainstream flue gas denitrification method in industrial boilers and power plants, the application of SCR into cement industry is very limited due to the problems of high dust content and complex components (e.g., alkali metals) in exhaust gas. Moreover, the extensive use of SCR into cement industry is also constrained by the development of low temperature catalysts [14–17].

To figure out the aforementioned bottleneck of existing denitrification technologies, an innovative NO_x reduction method, termed as fuel in-situ reduction (FISR), was developed and its feasibility had been confirmed using a pilot-scale experimental setup in our previous work [18, 19]. Different from the traditional process, the PC used for the precalciner in FISR method firstly experiences a pretreatment process and then enters the precalciner for combustion. Consequently, the factors affecting NO_x reduction and emission and their influence laws are also different in comparison to the traditional process when the pretreated fuel (PF) combusts in the precalciner. Obviously, it is unrealistic to study all these factors by means of experiments. As one of the primary methods studying the precalciner, numerical simulation technology can more efficiently and flexibly display the thermal process in the precalciner [20–23]. In the present work, with the pilot-scale precalciner in our previous work as the object, a series of numerical simulations were conducted to investigate the reduction and emission characteristics of NO_x with PF combusting in the precalciner by using ANSYS Fluent CFD software (version 18.1). The effects of initial NO and O_2 concentrations in kiln gas were clarified, and the optimal dimensionless positions of tertiary air-I and CRM feeding port were found. The results achieved in the present work can provide theoretical guidance for the optimization of FISR method in actual engineering application.

2. Principle and Application of FISR Method

Stimulating and improving the reduction capacity of carbon in reductive atmosphere is the key to the development of denitrification technologies in cement industry. In view of this, the combustion of PC coupled with pyrolysis and gasification has attracted more and more attention. Just under such background, FISR method was proposed and developed, and its schematic diagram is shown in Fig. 1.

Multistage cyclones (C_1–C_3) are ignored for simplicity. The PC used for the precalciner is first pretreated in a pretreater, which is designed to comply with the principle of circulating fluidized bed (CFB), and converted into PF, consisting of high-temperature syngas (HTSG) and pyrolysis semichar (PSC). In the pretreatment process, approximately 20%–40% of the theoretical air is injected into the CFB pretreater, and most of the fuel-N is volatilized and converted to N_2 in a strong reductive atmosphere, decreasing the possibility of the fuel-N oxidization. The HTSG primarily consists of N_2, CO_2, CO, H_2, and CH_4, which are ideal reducing agents except for the first two [24]. Besides, the PSC with bigger specific surface area and more extensive active sites than its parent coal, acting as a catalyst, would significantly accelerate the reaction between HTSG and NO_x [25].

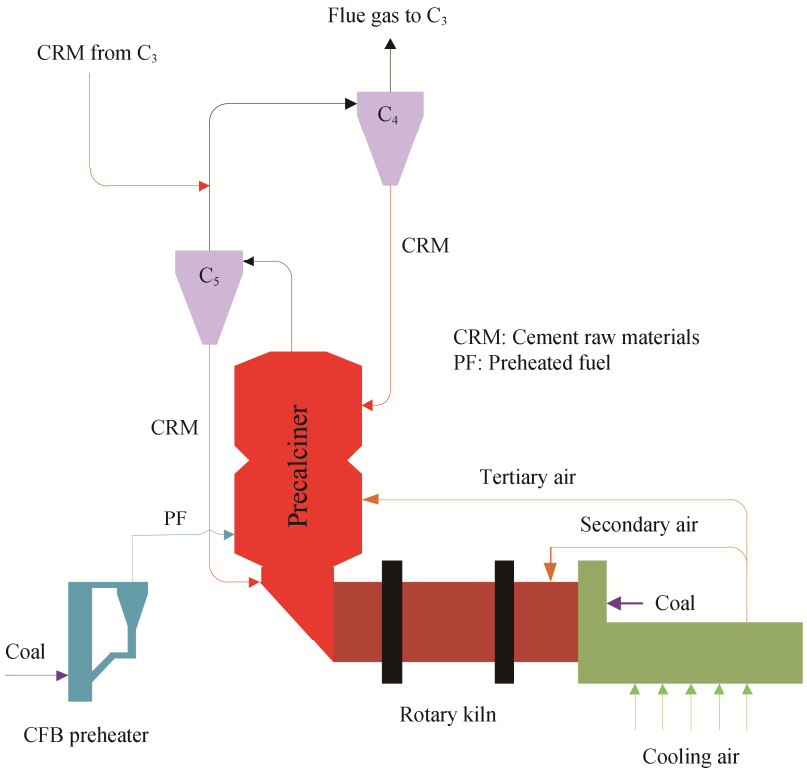

Fig. 1 Schematic diagram of FISR method

Table 1 Comprehensive comparison of FISR, SNCR and SCR method [19]

Method	Appraisal index			
	Initial investment/CNY	Operation cost/CNY	Secondary pollution	Denitrification efficiency/%
FISR	1 700 000	875 000	None	60–80
SCR	5 200 000	8 830 000	Ignored	90–95
SNCR	38 000 000	10 200 000	Ammonia escaped $(10–15)\times10^{-6}$ (in volume)	40–60

The PF replaces PC to enter the precalciner, and homogeneously and heterogeneously reacts with the NO_x in kiln gas by combining with air-staged combustion technology, and the reactions are described as follows (Eqs. (1)–(4)). Note that the real chemical reactions are significantly more complicated than the equations listed here [26, 27].

$$C+NO\rightarrow CO+1/2N_2 \quad (1)$$

$$CO+NO\rightarrow CO_2+1/2N_2 \quad (2)$$

$$CH_i+NO\rightarrow CO+N_2+OH+\ldots \quad (3)$$

$$H_2+NO\rightarrow H_2O+1/2N_2 \quad (4)$$

As mentioned above, the FISR method can theoretically reduce the NO_x of coal-fired cement kiln from two aspects: one is the pre-removal of fuel-N in the pretreatment process; the other is the stronger reducibility of PF than its parent coal.

At present, FISR method has been demonstrated and applied in a 2500 t/d cement production line in Ningxia and its denitrification efficiency reached 60%–80%. To demonstrate the technical and economic feasibility of the FISR method, the comprehensive comparison of FISR, SNCR and SCR technology on the identical cement production line is shown in Table 1 [19]. From technical and economic perspective, FISR is the most appropriate method for cement kiln system to cut NO_x emission.

3. Numerical Simulation

3.1 Mathematical model

3.1.1 Turbulent model

The RNG k-ε model is widely used to simulate the flows with swirling in engineering [28], and the general conservation equation of 3-D turbulent flow takes the form:

$$\frac{\partial}{\partial t}(\rho k)+\frac{\partial}{\partial x_i}(\rho k u_i)=\frac{\partial}{\partial x_j}\left(\alpha_k \mu_{\text{eff}}\frac{\partial k}{\partial x_j}\right)+G_k+G_b-\rho\varepsilon-Y_M+S_k \quad (5)$$

and

$$\frac{\partial}{\partial t}(\rho\varepsilon)+\frac{\partial}{\partial x_i}(\rho\varepsilon u_i)=\frac{\partial}{\partial x_j}\left(\alpha_\varepsilon\mu_{\text{eff}}\frac{\partial\varepsilon}{\partial x_j}\right)+C_{1\varepsilon}\frac{\varepsilon}{k}(G_k+C_{3\varepsilon}G_{\text{b}})-C_{2\varepsilon}\rho\frac{\varepsilon^2}{k}-R_\varepsilon+S_\varepsilon \tag{6}$$

in which

$$R_\varepsilon=\frac{C_\mu\rho\lambda^3(1-\lambda/\lambda_0)}{1+\beta\lambda^3}\frac{\varepsilon^2}{k} \tag{7}$$

Here, ρ is the density of the fluid. k is turbulence kinetic energy and ε is turbulent dissipation rate. u_i is the component of velocity in i direction. G_k represents the turbulence kinetic energy generation due to the mean velocity gradients. G_{b} is the turbulence kinetic energy generation due to the buoyancy. Y_M represents the contribution of the fluctuating dilatation in the compressible turbulence to the overall dissipation rate. $C_{1\varepsilon}$, $C_{2\varepsilon}$ and $C_{3\varepsilon}$ are constants, $C_{1\varepsilon}$=1.42, $C_{2\varepsilon}$=1.68. μ_{eff} is the turbulent viscosity. α_k and α_ε are the turbulent Prandtl numbers for k and ε, respectively. S_k and S_ε are user-defined source terms. $\lambda\equiv Sk/\varepsilon$, λ_0=4.38, β=0.012.

3.1.2 Discrete phase model

The volume fraction of PC or PSC solid particles in the precalciner is less than 10%, which makes that the particle phase trajectory can be calculated using the discrete phase model [29–31]. The particle dispersion due to turbulence in the fluid phase is predicted using the stochastic tracking model. For stochastic tracking, the discrete random walk model is adopted to account for the turbulence generation or dissipation in the gaseous phase. The particle trajectory is obtained by integrating the force balance on the particle, which is written in a Lagrangian reference frame. This force balance equates the particle inertia with the forces acting on the particle, and can be written (for the x direction in Cartesian coordinates) as:

$$\frac{\mathrm{d}u_{\text{p}}}{\mathrm{d}t}=F_{\text{D}}(u-u_{\text{p}})+\frac{g_x(\rho_{\text{p}}-\rho)}{\rho_{\text{p}}}+F_x \tag{8}$$

in which

$$F_{\text{D}}=\frac{18\mu}{\rho_{\text{p}}d_{\text{p}}^2}\frac{C_{\text{D}}Re}{24} \tag{9}$$

$$F_x=\frac{1}{2}\frac{\rho}{\rho_{\text{p}}}\frac{\mathrm{d}}{\mathrm{d}t}(u-u_{\text{p}}) \tag{10}$$

Here, the first term on the right-hand side, $F_{\text{D}}(u–u_{\text{p}})$, is the drag force per unit particle mass, and the second term, $g_x(\rho_{\text{p}}–\rho)/\rho_{\text{p}}$, denotes the gravity force. The last term F_x is an additional acceleration. u is the fluid-phase velocity. u_{p}, ρ_{p}, and d_{p} are velocity in the x direction, the density, and the diameter of the particle respectively. μ is hydrodynamic viscosity. C_{D} is drag coefficient and Re is particle Reynolds number.

3.1.3 Chemical reaction model

A species-transport model [32] is employed to calculate the chemical reactions, including homogeneous reactions of HTSG and heterogeneous reactions of PSC or PC particles. Since PSC particles still include certain volatiles, the reactions of PSC particles are the same as those of PC particles, which includes two steps: volatiles release and combustion, and residual-carbon-particle combustion.

The two-competing-rates model [33] is used to simulate the devolatilization. The model uses two first-order equations to control the reaction at low and high temperatures respectively, as follows:

$$R_1=A_1\mathrm{e}^{-(E_1/RT_{\text{p}})} \tag{11}$$

$$R_2=A_2\mathrm{e}^{-(E_2/RT_{\text{p}})} \tag{12}$$

where R_1 and R_2 are competitive devolatilization rates at low and high temperature ranges respectively. A and E are pre-exponential factor and activation energy of the reactions. R is molar gas constant and R=8.3145 J/(mol·K). The two rates are combined with different weighted values to form the expression of total devolatilization rate:

$$\frac{m_{\text{v}}(t)}{m_{\text{p},0}-m_{\text{a}}}=\int_0^t(\alpha_1R_1+\alpha_2R_2)\cdot\exp\left[-\int_0^t(R_1+R_2)\mathrm{d}t\right]\mathrm{d}t \tag{13}$$

Here, $m_{\text{v}}(t)$ is the sum of volatiles evaporated up to time t; $m_{\text{p},0}$ is the initial particle mass, and m_{a} is the mass of ash in the particle. α_1 and α_2 are the weighting factors of R_1 and R_2, respectively. The reaction kinetic data of devolatilization are listed in Table 2.

Table 2 Reaction kinetic data of volatiles devolatilization

Reaction	α	A/s^{-1}	E/J·kmol^{-1}
R_1	0.3	2.0×10^5	1.046×10^8
R_2	1	1.3×10^7	1.674×10^8

After devolatilization, the residual-carbon-particle is consumed by oxidation and gasification reactions, as shown in Table 3. The multiple-surface-reactions model [34, 35] is employed to simulate the heterogeneous process of char burnout.

Table 3 Reactions and kinetic data of residual-carbon-particle

Reaction	A/s^{-1}	E/J·kmol^{-1}
$C_{<s>}+1/2O_2\rightarrow CO$	0.001	6.248×10^7
$C_{<s>}+CO_2\rightarrow 2CO$	0.001	6.248×10^7
$C_{<s>}+H_2O\rightarrow CO+H_2$	0.001	6.248×10^7

3.1.4 Decomposition of CRM

In the present work, CRM is assumed to only consist of $CaCO_3$ and enters the precalciner at room temperature.

Finite rate-eddy dissipation model was used to simulate the decomposition of CRM, which is shown in Eq. (14). And the pre-exponential factor and activation energy of decomposition reaction are 2.47×10^6 s^{-1} and 1.236×10^8 J/kmol, respectively.

$$CaCO_3 \rightarrow CaO+CO_2 \quad (14)$$

3.1.5 NO_x formation and reduction

Since the amount of prompt-NO_x generally accounts for less than 5% of the total generated NO_x, only thermal-NO_x and fuel-NO_x are considered in the present work.

The formation of thermal-NO_x is determined by a set of highly temperature-dependent chemical reactions known as the extended Zeldovich mechanism [36]. The principal reactions governing the formation of thermal-NO_x from molecular nitrogen and the kinetic data for these reactions are listed in Table 4. The main factors affecting the formation of thermal-NO_x are flame temperature, high temperature range and oxygen concentration.

Table 4 Reactions for thermal-NO_x formation and expression of the rate coefficients [37]

Reaction	A/s^{-1}	E/J·$kmol^{-1}$
$O+N_2 \rightarrow N+NO$	1.8×10^8	3.19×10^8
$N+O_2 \rightarrow O+NO$	1.8×10^4	3.89×10^7
$N+OH \rightarrow H+NO$	7.1×10^7	3.74×10^6

For fuel-NO_x, although the route leading to fuel-NO_x formation and destruction is still not completely understood, different investigators seem to agree on a simplified model, as shown in Fig. 2. The nitrogen intermediates are grouped as HCN, NH_3, or a combination of both.

Fig. 2 The simplified model for the formation of fuel-NO_x

For the coal, it is assumed that fuel-N is distributed between the volatile and the char. In the present work, the pathway of fuel-NO_x is shown in Fig. 3.

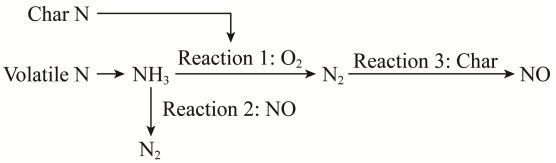

Fig. 3 Pathway of the formation for fuel-NO_x in the present work

Volatile-N is released in the form of NH_3, which is then oxidized to NO by O_2 (Reaction 1), and the unoxidized NH_3 will react with NO to form N_2 (Reaction 2). Char-N is directly oxidized to NO during the fuel combustion, and a portion of NO is reduced to N_2 on the char surface (Reaction 3). The kinetic data of the homogeneous reactions are shown in Table 5. The heterogeneous reaction of NO reaction on the char surface has been modeled according to the following:

$$R_3 = A_3 e^{-\left(E_3/R\overline{T}\right)} \overline{p}_{NO} \quad (15)$$

where R_3 is the reaction rate of NO reduction, with the unit of mol/(m^2·s). $\overline{p}_{NO}$ is the mean NO partial pressure, with the unit of Pa. $\overline{T}$ is the mean temperature, with the unit of K. The pre-exponential factor and activation energy of the heterogeneous reaction are 2.27×10^{-3} mol/(m^2·s·Pa) and 1.43×10^8 J/kmol, respectively. The char suface area is obtained using the BET test method.

Table 5 Kinetic data for the homogeneous reactions [38] in Fig. 3

Reaction	A/s^{-1}	E/J·$kmol^{-1}$
1	4.0×10^6	1.34×10^8
2	1.8×10^8	1.13×10^8

The instantaneous NO_x reburning mechanism is a pathway whereby NO reacts with hydrocarbons and is subsequently reduced. Three reburn reactions are modeled by ANSYS Fluent when the temperature is between 1600 K and 2100 K. The reactions and kinetic data are listed in Table 6.

Table 6 Reactions and kinetic data for NO_x reburning mechanism [39]

Reaction	A/s^{-1}	E/J·$kmol^{-1}$
$CH+NO \rightarrow HCN+O$	1×10^8	–
$CH_2+NO \rightarrow HCN+OH$	1.4×10^6	4.57×10^6
$CH_3+NO \rightarrow HCN+H_2O$	2×10^5	-

The turbulence interaction effect is considered by using the β-PDF (Probability Density Function) model. Since the amount of NO_x is small, it does not affect the flow field, temperature field and concentration field of main components in the precalciner. Therefore, NO_x formation and reduction is studied using a post-processing approach [40].

3.2 Geometrical model and mesh

The precalciner is a three-sprayed precalciner, with the height of 7.5 m and the inner diameter of 0.174 m, which is split into three parts: upper, middle, and lower. And the two ends of the middle part are respectively provided with a necking pipe to enhance blending [18, 19]. The geometry is established according to the actual size of 1:1, as shown in Fig. 4. A Cartesian coordinate system is set at the center of the interface between the cone and straight of the lower part, and the positive direction of Z

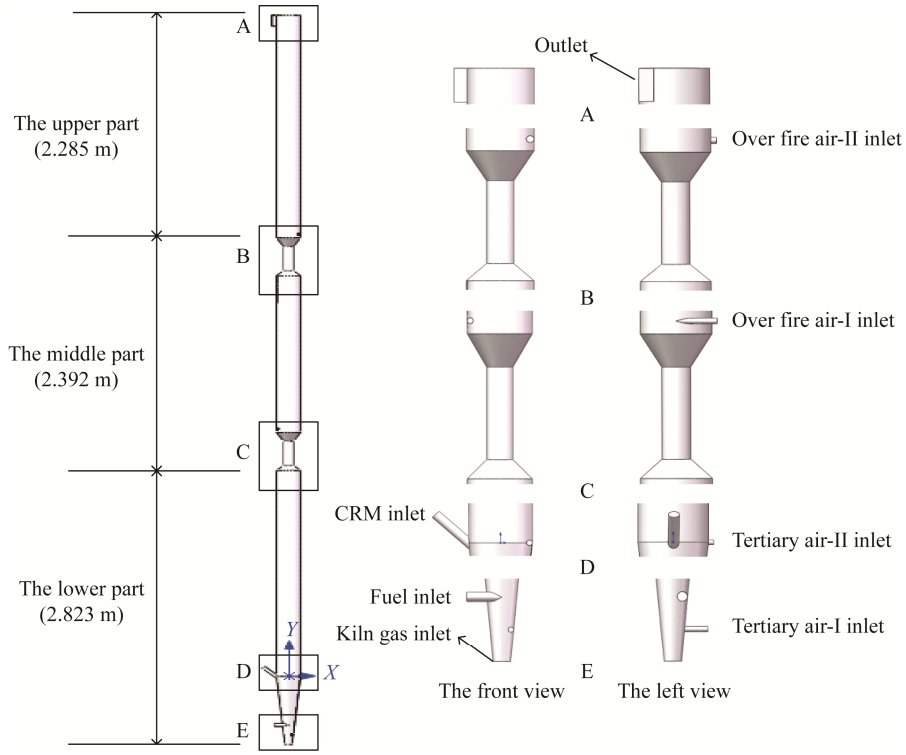

Fig. 4 Geometrical model of the precalciner

axis is perpendicular to the paper surface outward. Therefore, the height range of the precalciner Y is –0.7 m to 6.8 m. Kiln gas vertically enters the precalciner from the bottom inlet with a diameter of 50 mm. The fuel inlet is located at Y=–0.5 m, with a counterclockwise incident direction (from the top view, same as below) and a diameter of 29 mm. Four stages of air-staged combustion scheme are adopted. Tertiary air-II, over-fire air-II were injected in counterclockwise at Y=0 m, 4.55 m respectively, while over-fire air-I was introduced to the precalciner in clockwise at Y=2.55 m. The location of tertiary air-I varies from Y= –0.6 m to Y=0 m for the optimization study. Except that the diameter of over-fire air-II inlet is 10 mm, the diameters of other staged-air inlets are 16 mm. The location of CRM inlet with a diameter of 27 mm varies from Y= –0.6 m to Y=0.6 m in the simulation. And there is an rectangular tangential outlet at the top side of the precalciner, with a height of 110 mm and a width of 37 mm. The various inlet boundaries are simplified to facilitate meshing, and the whole computational domain consists of a structured hexahedral mesh with 540 thousand cells (see Section 3.4 for the grid independence test).

3.3 Calculation settings

The specific boundary conditions for various inlets and solid walls of all cases are listed in Table 7. The boundary conditions used to verify the accuracy and reliability of the present model were consistent with the experimental data in our previous work [18]. It's worth noting that, in order to compare NO_x emission levels of PC and PF (see Section 4.2), the thermal processes of two fuels were respectively simulated with the same boundary conditions except the fuel inlet. When applying FISR method, PC with a mass flow rate of 0.001 067 kg/s (3.84 kg/h) and air with stoichiometric ratio of 0.4 were fed into the CFB pretreater, and then the PF (consisting of HTSG and PSC) produced in pretreatment process entered the precalciner through the fuel inlet for the combustion. When PC directly combusts in the precalciner, the above PC and air were sent to the precalciner through the fuel inlet for the combustion.

The air-staged schemes in all cases were the same to minimize the variation of flow field in the precalciner. And the stoichiometric ratios of each stage air are defined as follows:

$$\alpha_{\text{TA-I}} = \frac{Q_{\text{TA-I}}}{L^0} \tag{16}$$

$$\alpha_{\text{TA-II}} = \frac{Q_{\text{TA-II}}}{L^0} \tag{17}$$

$$\alpha_{\text{OF-I}} = \frac{Q_{\text{OF-I}}}{L^0} \tag{18}$$

$$\alpha_{\text{OF-II}} = \frac{Q_{\text{OF-II}}}{L^0} \tag{19}$$

where $\alpha_{\text{TA-I}}$, $\alpha_{\text{TA-II}}$, $\alpha_{\text{OF-I}}$ and $\alpha_{\text{OF-II}}$ are the stoichiometric ratios of Tertiary air-I, Tertiary air-II, Over fire air-I and

Table 7 Boundary conditions for various inlets and solid walls of all cases

Boundary		Species/ vol%	Velocity/ $m \cdot s^{-1}$	Mass flow rate/ $kg \cdot s^{-1}$	Temperature/ K
Fuel inlet	PC combusts in the precalciner	O_2: 21 N_2: 79	5.47 (Air)	0.001 067 (PC particles)	293
	PF combusts in the precalciner	CO_2: 13.33 CO: 6.94 CH_4: 3.02 H_2: 4.82 N_2: 71.89	18.13 (HTSG)	0.000 417 (PSC particles)	948
Kiln gas inlet		O_2: 3, 4, 5, 6, 7 CO_2: 8.79 H_2O: 11.72 N_2: 4.36 NO: 0.07, 0.08, 0.09, 0.10, 0.11, 0.12 (with NO in kiln gas)	16.40	–	1323
CRM inlet		$CaCO_3$: 100	–	0.011 111	293
Tertiary air-I inlet		O_2: 21 N_2: 79	10.50	–	293
Tertiary air-II inlet			1.870		
Over fire air-I inlet			10.77		
Over fire air-II inlet			25.06		
Wall		–	–	–	Upper: 993
		–	–	–	Middle: 1093
		–	–	–	Lower: 1173 (cylinder) 1073 (cone)

Table 8 Proximate and ultimate analysis results of PC and PSC

Items	Proximate analysis/wt%, ar				Ultimate analysis/wt%, ar					Lower heating value/$kJ \cdot kg^{-1}$
	Moisture	Ash	Volatile	Fixed carbon	Carbon	Hydrogen	Oxygen	Nitrogen	Sulfur	
PC	6.00	6.60	32.26	55.13	70.56	4.34	11.33	0.88	0.29	27.04
PSC	1.40	16.87	9.00	72.73	77.65	1.40	1.06	1.31	0.31	27.65

Table 9 Particle size and specific surface area of PC and PSC

Sample type	D_{10}/μm	D_{50}/μm	D_{90}/μm	Specific surface area/$m^2 \cdot g^{-1}$
PC	29.072	151.180	344.202	0.103
PSC	9.419	91.059	209.835	0.221

Over fire air-II, respectively. $Q_{TA\text{-}I}$, $Q_{TA\text{-}II}$, $Q_{OF\text{-}I}$ and $Q_{OF\text{-}II}$ are the volume flow rates of Tertiary air-I, Tertiary air-II, Over fire air-I and Over fire air-II, respectively, with the unit of m^3/h at 273 K, 101 325 Pa. L^0 is the theoretical combustion air demand, with the unit of m^3/h, at 273 K, 101 325 Pa. The value of $\alpha_{TA\text{-}I}$, $\alpha_{TA\text{-}II}$, $\alpha_{OF\text{-}I}$ and $\alpha_{OF\text{-}II}$ are 0.27, 0.04, 0.27 and 0.24, respectively. Therefore, the lower part is the reduction zone in the precalciner.

The proximate and ultimate analysis results of PC and PSC are listed in Table 8. The size distributions of PC and PSC conform to Rosin-Rammmer distribution, and the vital parameters of the particle size and specific surface are listed in Table 9. A full developmental flow was adopted for the outlet of the precalciner.

Convection and diffusion of the conservation equations were discretized with the volume finite method. The Semi-Implicit Method for Pressure Linked Equations (SIMPLE) method was employed to combine pressure and velocity calculations. All the equations were computed with low relaxation factors and iteration of the Tridiagonal matrix algorithm. The convergence criterion for the residuals of the continuity, energy and radiation equation was less than 10^{-6}, and less than 10^{-3} for the remaining residuals, and the deviation of energy inflow and outflow was within 0.1%.

3.4 The independence tests

In order to verify the independence of simulation results, we conducted the simulations under the same working conditions when the grid numbers were 540 thousand, 1.05 million, and 1.52 million respectively. The average temperature of the cross-section every 0.1 m along the axis of the precalciner was selected for the comparison. The temperature profiles under the different grid numbers are shown in Fig. 5. The differences of computational results among three kinds of grids were within –2.06% to 2.58%. Considering the time cost of the calculation, the 540 thousand-grid simulation was employed in the following research.

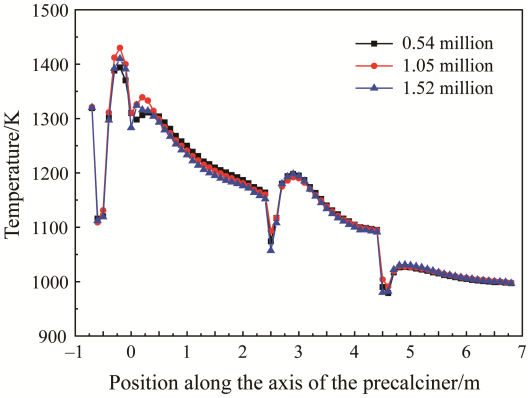

Fig. 5 The grid independence tests

4. Results and Discussion

4.1 Model verification

In order to validate the present model, we conducted a comparison between experimental data [18] and simulation results for ten temperature sampling points when PF burns in the percalciner, as shown in Table 10. The maximum deviation is 9.27% and the minimum one is –0.09%. Considering the diversity of gas composition, complexity of chemical reaction, and thermal insulation performance of the precalciner, the deviation between measurement data and simulation results is within an acceptable range. On the whole, the numerical simulation results are in good agreement with the experimental data, which indicates the present model is reliable.

Table 10 Comparison between experimental data and simulation results for ten temperature sampling points

Y/m	–0.4	0.45	0.95	1.95	2.65
Experimental data/K	1110	1218	1255	1162	1090
Simulation data/K	1157	1268	1207	1172	1191
Deviation/%	+4.23	+4.10	–3.82	+0.86	+9.27
Y/m	3.55	4.05	5.05	6.05	6.75
Experimental data/K	1122	1092	1151	972	932
Simulation data/K	1126	1091	1052	1000	992
Deviation/%	+0.35	–0.09	–8.60	+2.88	+6.44

Except for the ten temperature sampling points, NO_x emission concentration at the outlet of the precalciner is also selected to validate the reliability of the model, expressed as:

$$[NO_x]_{mc,precalciner} = \frac{46}{22.4} \times [NO]_{vc,precalciner} \times \frac{21\% - 10\%}{21\% - [O_2]} \quad (20)$$

where $[NO]_{vc,precalcier}$, with the unit of 10^{-6} (in volume), is the volume concentration of NO at the outlet of the precalciner, and $[O_2]$ means the real measuring or simulating oxygen content at the outlet of the precalciner with the unit of %. $[NO_x]_{mc,precalciner}$, with the unit of mg/m^3, refers the converted mass concentration of NO_x at the outlet of the precalciner in terms of 10% oxygen content according to Chinese National Standard (GB4915-2013). According to Eq. (20), the simulation value of $[NO_x]_{mc,precalciner}$ is 144.66 mg/m^3 while the experimental value is 137.96 mg/m^3 under the same conditions [18]. The deviation is 4.68%, which indicates the reliability of the present model again. Note that all the mass concentrations of NO_x involved in this paper are obtained by means of Eq. (20) according the corresponding volume concentration and oxygen content.

4.2 Comparison of NO_x emission for PC and PF combusting in the precalciner

No matter whether the fuel is PC or PF, a part of NO in kiln gas can be reduced by the fuel. In order to quantitatively observe the reduction effects of different fuels, an index was introduced to characterize the reduction rate of NO in kiln gas, expressed as:

$$\eta = \frac{[NO]_{vc,kiln} \times \beta - \left([NO]^1_{vc,precalciner} - [NO]^0_{vc,precalciner}\right)}{[NO]_{vc,kiln} \times \beta} \quad (21)$$

where $[NO]_{vc,kiln}$, with the unit of 10^{-6} (in volume), denotes the volume concentration of NO in kiln gas. $[NO]_{vc,precalciner}$ is the volume concentration of NO at the outlet of the precalciner, and the superscript "1" means that the kiln gas contains NO, i.e., NO at the precalciner outlet comes from two sources: kiln gas and combustion of fuel in the precalciner. The superscript "0" represents the case without NO in kiln gas, i.e., NO only originates from the combustion of fuel. β is the dilution coefficient, which characterizes the dilution effect of flue gas (generated due to the combustion of fuel and decomposition of CRM in the precalciner) on NO concentration, and its value is the ratio of kiln gas to total flue gas (volume ratio). From Eq. (21), it can be seen that both dilution effect of the flue gas and nitrogen oxide generated due to the combustion of fuel in the precalciner are considered when calculating the reduction rate.

Noting that the feeding amount of CRM was 0, i.e., CRM and its decomposition were not considered in this section (the same treatment in Section 4.3, and β was within 0.3997–0.4147 under this condition). Since the fuel inlet is located at Y= –0.5 m, the difference of the two thermal processes is mainly reflected in the lower part. Fig. 6 illustrates the mass concentration distribution of NO_x with cross section of Z=0 in this range. Comparing Fig. 6(a) with 6(b), without NO in kiln gas, the NO_x concentration of PF combustion process is obviously lower than that of PC, and the low concentration region of NO_x in the former is concentrated

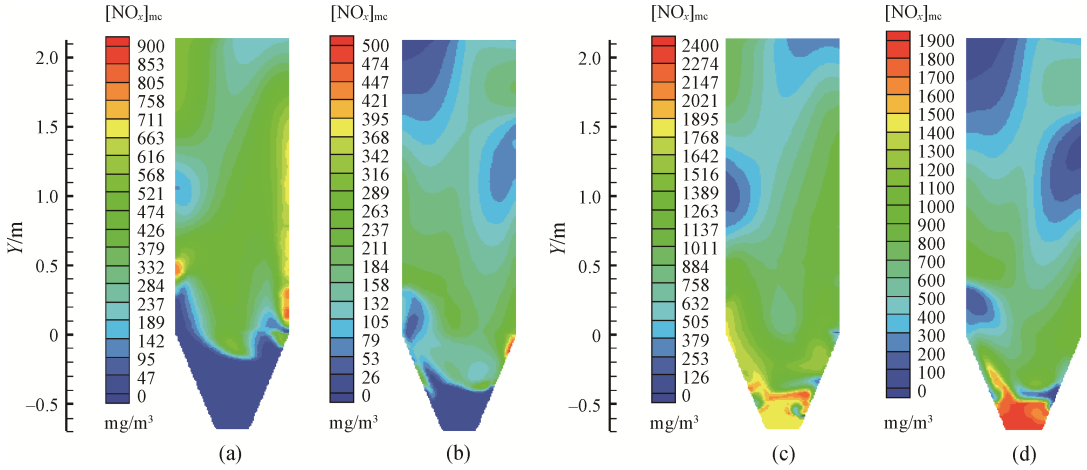

Fig. 6 Mass concentration distribution of NO_x with cross section of Z=0 in the lower part (obtained by means of Eq. (15) according the corresponding local [NO] and [O_2], the same as below). (a) PC in the precalciner without NO in kiln gas; (b) PF in the precalciner without NO in kiln gas; (c) PC in the precalciner with 1.2×10^{-3} (in volume) NO in kiln gas; (d) PF in the precalciner with 1.2×10^{-3} (in volume) NO in kiln gas

in the cone, while that of the latter is scattered in the whole lower part. When PC is burned in the precalciner, cold PC and air need to be heated before burning. However, PF with a temperature of 948 K can be burned quickly after entering the precalciner, so the position of NO_x generated in the combustion process of PC is higher than that of PF. The lower NO_x concentration in the PF combustion process is due to the conversion of fuel-N to N_2 during pretreatment process.

When there is NO in kiln gas, the low-concentration area of NO_x in Fig. 6(c) and 6(d) basically coincides with Fig. 6(a) and 6(b), respectively. The area with the highest NO_x concentration in Fig. 6(c) is around Y=–0.4 m, while that in Fig. 6(d) is at the entrance of the kiln gas. After PC enters the precalciner at Y=–0.5 m, fuel-N separates out with volatilization in the heating process of PC, and is oxidized to NO_x, making NO_x concentration the highest at Y= –0.4 m. As the combustion and NO_x reduction reactions proceed, NO_x concentration decreases at the position above Y=–0.4 m. However, owning to the stronger reducibility of PF than PC, PF can reduce the NO in kiln gas after entering the precalciner. Besides, the PSC with bigger specific surface area and more extensive active sites, acting as a catalyst, significantly accelerates the reduction of NO_x, which is the reason why there are more low concentration areas of NO_x in Fig. 6(d).

Fig. 7 shows the NO_x emission and reduction rate of NO in the two thermal processes. The concentration of NO_x originates from the combustion of PC is 286 mg/m^3 while the value for PF is only 46.93 mg/m^3. With 1.2×10^{-3} (in volume) NO in kiln gas, the NO_x emission concentration are 479.98 mg/m^3 and 144.66 mg/m^3, and the reduction rate of NO are 69.35% and 84.71%, respectively, for PC and PF combustion in the precalciner. The results demonstrate that the NO_x generated in the

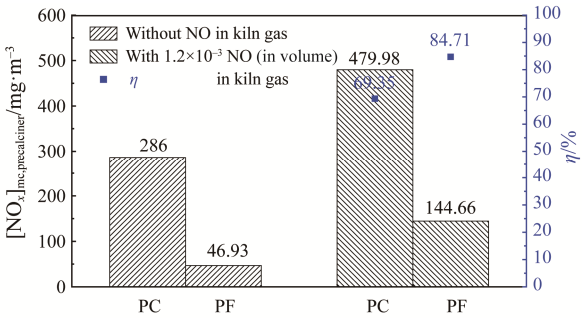

Fig. 7 Comparison of NO_x emission and reduction rate of NO in kiln gas for the two fuels

combustion process can be reduced by 83.59%, and the reduction rate of NO can be increased by 22.15% after FISR method is adopted. In addition, due to the difference of fuel inlet boundary conditions, the residence time of flue gas in the reduction zone (abbreviated as "residence time" and represented by the symbol "t" in the following text) during PF combustion (1.473 s) is slightly shorter than that during PC combustion (1.694 s), which further indicates the strong reducibility of PF.

4.3 Low NO_x emission for PF combusting in the precalciner

NO generated in the rotary kiln gas due to high-temperature combustion is the mainly source of NO_x emissions, which indicates the initial NO concentration in kiln gas has an important influence on the NO_x emission at the precalciner's outlet. The oxygen content in kiln gas is another factor affecting the NO_x emission because it is related the NO reduction. Of course, when the TSC technology is employed, the location of tertiary air-I has a more significant and direct

impact on the NO reduction by affecting the flow filed and oxygen distribution. Therefore, it is quite necessary to study the influence of above-mentioned factors on the denitrification effect of FISR method. Noting that the CRM and the decomposition of CRM are not considered in all cases in this section.

4.3.1 The effect of initial NO concentration in kiln gas

For the actual cement kiln, NO concentration in kiln gas is generally within 7.5×10^{-4}–12×10^{-4} (in volume, the same for the following gas concentration). In view of this, a series of simulations were conducted for different initial NO concentrations, i.e., 7×10^{-4}, 8×10^{-4}, 9×10^{-4}, 10×10^{-4}, 11×10^{-4} and 12×10^{-4}. The content of O_2 in kiln gas was fixed at 5% for all simulation cases. As shown in Fig. 8, with increasing the initial NO concentration, the NO_x emission concentration increases linearly, while the reduction rate has only a slight decrease from 85.72% to 84.27%. From the data, the initial NO concentration increases by 71.43% (from 7×10^{-4} to 12×10^{-4}), while the NO_x emission increases by 46.57% (from 98.7 mg/m^3 to 144.66 mg/m^3). This implies that, the total amount of NO reduced in the precalciner increases although the initial NO concentration rises. It demonstrates that the PF obtained by the pretreatment process has a strong reducibility. Above 80% reduction rate of NO ensures that even if the initial concentration of NO in kiln gas reaches 12×10^{-4}, the final emission of NO_x can be still maintained at a relatively low level (144.66 mg/m^3). In the case of 7×10^{-4}, the NO_x emission concentration of 98.7 mg/m^3 has reached ultra-low emission level. According to Chinese National Standard (GB4915-2013), NO_x emission limit of cement kiln is 400 mg/m^3 for general areas and 320 mg/m^3 for key areas. Without ammonia injection, NO_x emission can be controlled far below the standard limit by adopting FISR method, which demonstrates that this new-type method has broad application prospects and advantages compared with the existing denitrification technologies (e.g. SNCR). It should be noted that, although FISR method has a high reduction rate of NO, a low NO concentration in kiln gas is still desired to realize a lower emission of nitrogen oxides.

4.3.2 The effect of O_2 content in kiln gas

In order to form a stable and ideal flame and achieve effective combustion in rotary kiln, excess air is usually required. Normally, oxygen content in kiln gas is controlled below 3.0% according to the requirements of cement production. However, the actual O_2 concentration in kiln gas is quite different for various cement production lines in China, varying from 0 vol% to 15 vol%. In view of this, several typical O_2 concentrations, i.e., 3%, 4%, 5%, 6% and 7% were used to study the effect of oxygen content in kiln gas on NO_x emission in the present simulation. The initial NO concentration was fixed at 12×10^{-4} for those cases with NO in kiln gas. As shown in Fig. 9, when O_2 concentration rises from 3% to 7%, the mass concentration of NO_x solely generated by the combustion of PF in the precalciner increases from 15.15 mg/m^3 to 97.99 mg/m^3 (i.e., cases without NO in kiln gas), which indicates that too high oxygen concentration in kiln gas will promote the conversion of fuel-N in PF to nitrogen oxides. When kiln gas contains 12×10^{-4} NO, the NO_x emission increases from 42.48 mg/m^3 to 295.44 mg/m^3 with increasing oxygen content from 3% to 7%. Correspondingly, the reduction rate of NO dramatically decreases from 96.61% to 71.13%. Thus it can be seen that, in addition to affecting the conversion of fuel-N, too high oxygen concentration in kiln gas will also weaken the reduction of NO by the PF. The above two reasons lead to high NO_x emission under the condition of high oxygen content in kiln gas. When oxygen content in kiln gas is more than 4%, the negative effect of oxygen on NO_x emission and reduction rate are more obvious. For actual large cement kiln, the O_2

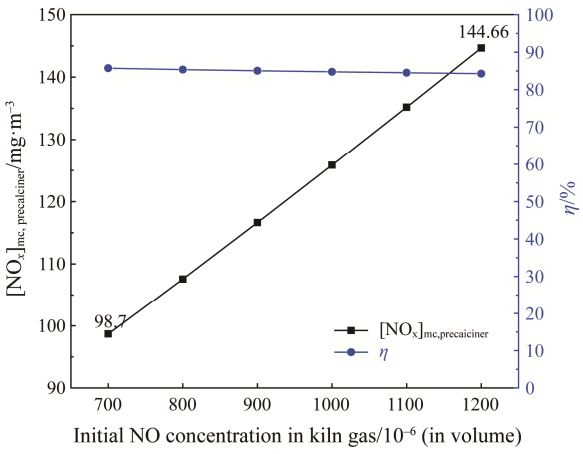

Fig. 8 Effect of the initial NO concentration in kiln gas on the NO_x emission and reduction rate

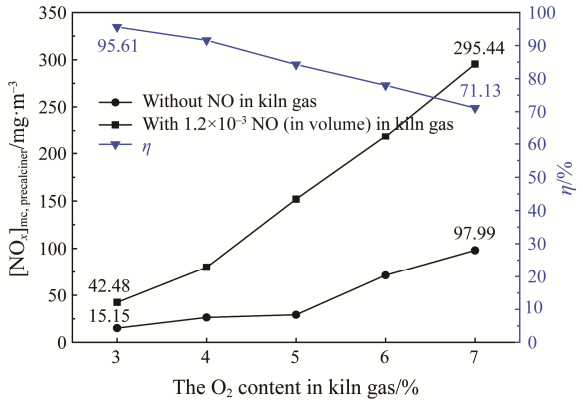

Fig. 9 Effect of O_2 concentration in kiln gas on the NO_x emission and reduction rate

concentration needs to satisfy both the calcination temperature of clinker in rotary kiln and NO_x reduction in the precalciner. Therefore, the O_2 concentration in kiln gas should be as small as possible on the premise of ensuring the temperature in rotary kiln when FISR method is applied in the actual engineering.

4.3.3 The effect of tertiary air-I inlet location

In order to better guide the application of FISR method, a dimensionless location of tertiary air-I was defined as:

$$Y^*_{\text{TA-I}} = \frac{Y_{\text{TA-I}} - Y_{\text{fuel}}}{|Y_{\text{fuel}}|} \tag{22}$$

where $Y^*_{\text{TA-I}}$ refers to the dimensionless location of tertiary air-I inlet. $Y_{\text{TA-I}}$ and Y_{fuel} represent the actual locations of tertiary air-I inlet and fuel inlet, respectively, with the unit of m. According to the structure of the precalciner, $Y_{\text{fuel}} = -0.5$ m. In view of the engineering practice, $Y^*_{\text{TA-I}}$ was set to –0.2, 0, 0.2, 0.4, 0.6, 0.8, and 1.0 in the present simulation (corresponding to $Y_{\text{TA-I}}$ = –0.6 m, –0.5 m, –0.4 m, –0.3 m, –0.2 m, –0.1 m, and 0 m). The O_2 content in kiln gas was fixed at 5%, and the initial NO concentration was set at 12×10^{-4} for those cases with NO in kiln gas.

According to the simulation results, the distinction of NO_x mass concentration distribution with cross section of Z=0 among different $Y^*_{\text{TA-I}}$ is mainly reflected in the lower part of the precalciner, as shown in Fig. 10. For $Y^*_{\text{TA-I}} = -0.2$, the inlet for tertiary air-I is located below that of PF. Therefore, tertiary air-I needs to pass a certain distance before encountering the fuel, and PF moves a long distance in the lower part due to the entrainment of the gas flow. As a result, NO_x generated by the combustion of PF is widely distributed throughout the lower part. For $Y^*_{\text{TA-I}}$=0, both the inlets of tertiary air-I and PF are located at the same position, i.e., Y=–0.5 m, which implies that tertiary air-I and PF meet and burn instantaneously after entering the precalciner. Hence, compared with $Y^*_{\text{TA-I}}$= –0.2, the NO_x concentration distribution is more concentrated and the distribution range is smaller when $Y^*_{\text{TA-I}}$=0. For $Y^*_{\text{TA-I}}$>0, the inlet of tertiary air-I moves up above that of PF, and tertiary air-I entering the precalciner horizontally tangentially intercepts PF laterally, so that NO_x generated is mainly distributed in the range of Y= –0.5 m to 0.5 m. As a whole, it is favorable for the conversion of fuel-N to N_2 that the inlet of tertiary air-I moves up in a certain range.

On the other hand, the change of tertiary air-I inlet also greatly affects the reduction of NO from kiln gas, as shown in Fig. 10(b). When the inlet of tertiary air-I is below that of PF (i.e., $Y^*_{\text{TA-I}}$<0), the reduction of NO by the reductant in PF is severely weakened due to the

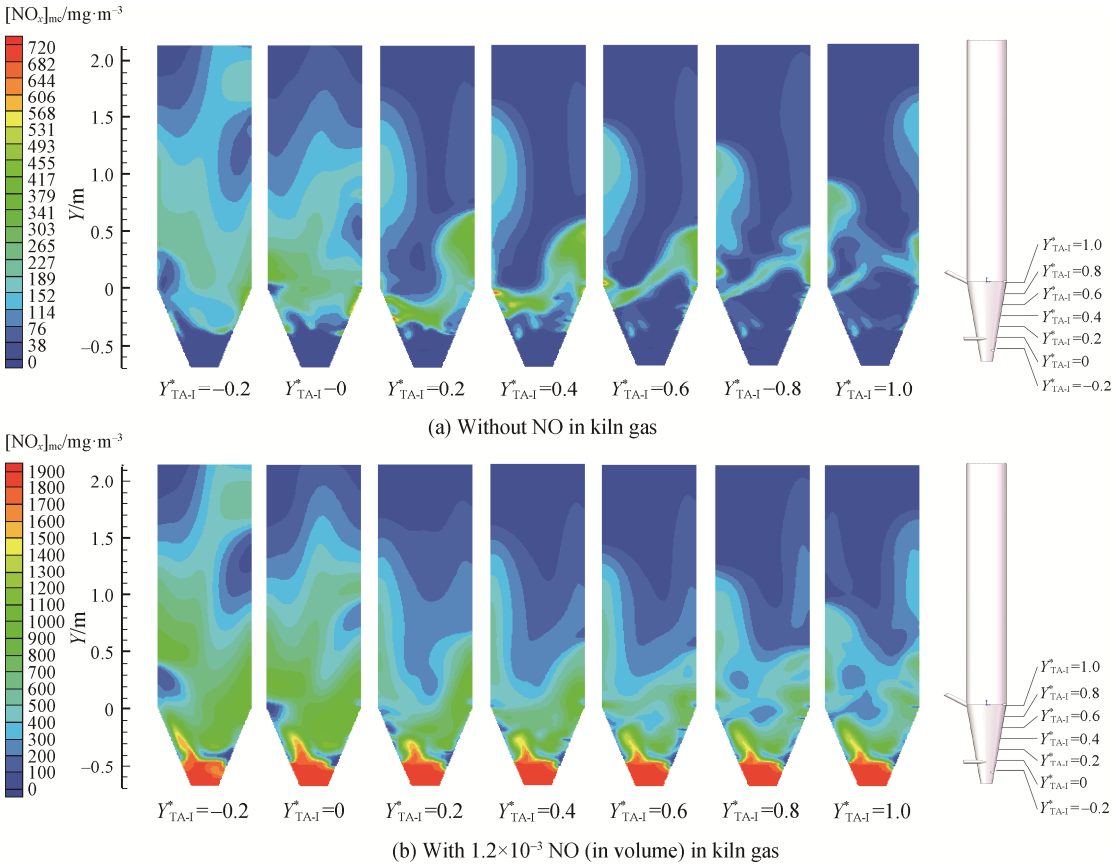

Fig. 10 Mass concentration distribution of NO_x (section Z=0) in the lower part of the precalciner for different $Y^*_{\text{TA-I}}$

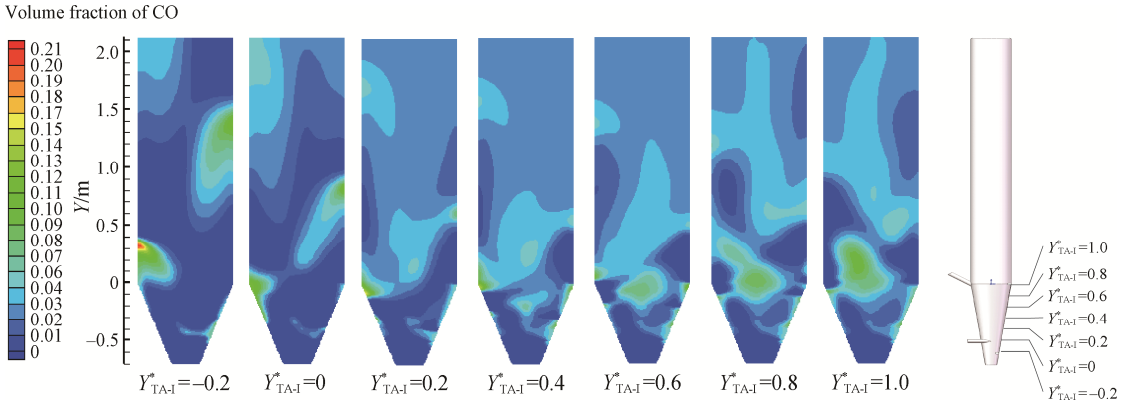

Fig. 11 Volume fraction of CO (section Z=0) in the lower part of the precalciner for different Y^*_{TA-I}

early emergence of air. As the inlet of tertiary air-I moves up, the reduction of NO is gradually strengthened thanks to the expansion of zone with reducing atmosphere. When Y^*_{TA-I}=0.2, most of NO in kiln gas can be reduced in the range of Y<2 m. With the further increase of Y^*_{TA-I}, NO in kiln gas is reduced earlier, which makes that the region with high NO_x concentration is compressed. Essentially, the distribution of NO_x in the precalciner is mainly determined by the distribution of reductants (semichar, CO, etc.). Fig. 11 shows the volume concentration distribution of CO with cross section of Z=0 in the lower part of the precalciner under different Y^*_{TA-I} values. It can be found that, when Y^*_{TA-I}>0, the distribution of CO is more uniform than that in the case of Y^*_{TA-I}<0, which is conducive to the reduction of NO in kiln gas.

Fig. 12 displays the NO_x emission, NO reduction rate and residence time under different Y^*_{TA-I}. When Y^*_{TA-I} increases from –0.2 to 0.2, both NO_x emission and reduction rate experience important changes, while residence time varies slightly. The NO_x emission concentration decreases by 74.6% (from 144.66 mg/m^3 to 36.81 mg/m^3), and the reduction rate of NO_x increases by 14% (from 84.7% to 96.57%). With further increasing Y^*_{TA-I}, although residence time gradually lengthens, both NO_x emission and reduction rate change little in general

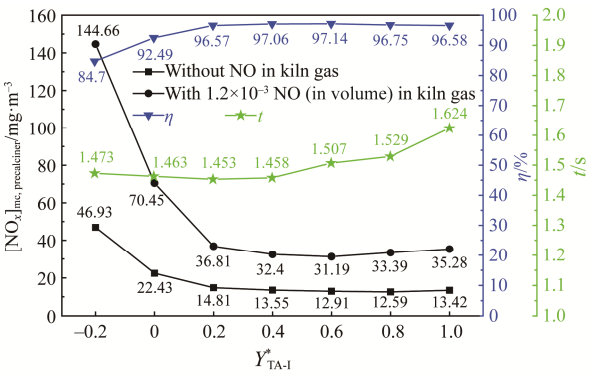

Fig. 12 Effects of Y^*_{TA-I} on the NO_x emission, reduction rate and residence time

because the reduction potential has been fully exploited. According to the present simulation results, the optimal Y^*_{TA-I} value is 0.6 where NO_x emission reaches the minimal value (31.19 mg/m^3) and the reduction rate achieves the peak value (97.14%). In the practical engineering application, once the entrance of PF is confirmed, the optimal location of tertiary air-I can be determined according to Eq. (22).

4.4 The coupling process of PF combustion and CRM decomposition in the precalciner

The combustion reactions of PF are coupled with the decomposition of CRM in the actual engineering and they interact with each other. Ensuring the burn-out rate of fuel and the decomposition rate of CRM is an important prerequisite for the structural design and operation of the precalciner. Therefore, the combustion of PF in the presence of CRM was simulated to observe the effect of CRM decomposition on NO_x emission. According to the ratio of CRM to fuel (mass ratio) in the practical cement kiln, the feeding rate of CRM with atmospheric temperature is set as 0.011 kg/s (about 40 kg/h). Both oxygen content and NO concentration in kiln gas are the same as those in Section 4.3.3. In order to further investigate the effect of CRM inlet location and make the results more universal, a dimensionless variable was defined as

$$Y^*_{CRM} = \left| \frac{Y_{CRM} - Y_{TA-I}}{Y_{fuel}} \right| \tag{23}$$

where Y^*_{CRM} refers to the dimensionless location of CRM inlet. Y_{TA-I} and Y_{fuel} are fixed at –0.6 m and –0.5 m, respectively. In view of the practical engineering, seven Y^*_{CRM} values, i.e., 0, 0.4, 0.8, 1.2, 1.6, 2.0 and 2.4, were chose for the simulation, corresponding to Y_{CRM} = –0.6 m, –0.4 m, –0.2 m, 0 m, 0.2 m, 0.4 m and 0.6 m.

4.4.1 NO_x emission in the presence of CRM

Fig. 13 shows the mass concentration distribution of NO_x with cross section of Z=0 (in the lower part of the precalciner) in the presence of CRM when Y^*_{CRM}=1.2

(Y_{CRM}=0 m). Compared with those cases without CRM, the overall concentration distributions of NO_x are lower, and the region with low NO_x concentration is also been enlarged. Two reasons should be responsible for this phenomenon. When considering the existence of CRM, the overall temperature in the precalciner is lower due to the absorption of sensible heat and reaction heat for CRM, which is beneficial to reduce the formation of NO_x generated by the combustion of PF. Besides, the feeding of CRM can not only affect the flow field in the precalciner, but bring about the dilution effect due to the increase of flue gas (The decomposition of CRM produces a lot of carbon dioxide). It should be noted that CRM can also affect the formation and reduction of NO_x as the particle carrier of homogeneous reaction [41]. Nevertheless, there is no relevant model to describe this effect so far.

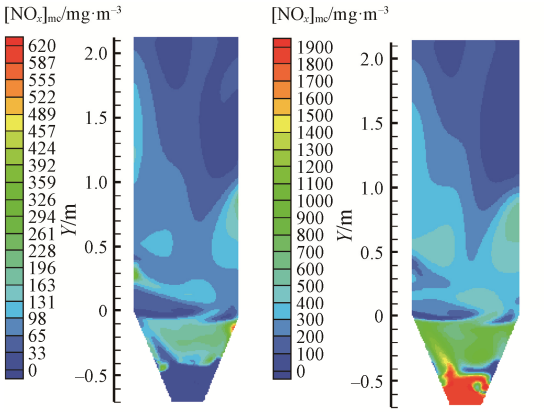

(a) Without NO in kiln gas (b) With 1.2×10^{-3} NO (in volume) in kiln gas

Fig. 13 Mass concentration distribution of NO_x (Z=0) in the lower part of the precalciner

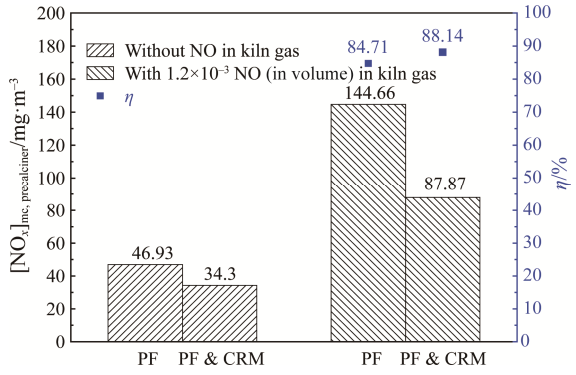

Fig. 14 Comparison of NO_x emission and reduction rate in the absence and presence of CRM

Fig. 14 shows the comparison of NO_x emission and reduction rate in the absence and presence of CRM. For the case without NO in kiln gas, NO_x emission decreases by 27.3% (from 46.93 mg/m^3 to 34.3 mg/m^3) after adding CRM, while the decreasing magnitude of NO_x emission reaches 39.3% (from 144.66 mg/m^3 to 87.87 mg/m^3) for the case with 12×10^{-4} NO in kiln gas. And the reduction rate of NO_x increases from 84.71% to 88.14% in the presence of CRM (noting that β is within 0.3043–0.3060 in the presence of CRM).

4.4.2 The effect of CRM inlet location

As mentioned above, the addition of CRM can affect the flow field, temperature filed and component concentration field in the precalciner, and thereby influence the formation and reduction of NO_x. The location of CRM inlet is the decisive factor of above effects. Therefore, it is necessary to explore the optimum location of the CRM inlet. Fig. 15 shows the mass concentration distribution of NO_x with cross section Z=0 for different Y^*_{CRM}. When Y^*_{CRM} =0, CRM enters the precalciner below the PF, and then moves upward together with PF. Owing to the heat absorption of CRM, the temperature in the precalciner decreases, which causes the delay of preheated fuel combustion. Consequently, the initial position of NO_x formation also moves up. For Y^*_{CRM}=0.4 and 0.8, CRM inlet is located above fuel inlet. Before encountering CRM, PF has burned due to the supply of tertiary air-I, which weakens the cooling effect of CRM. Therefore, the initial position of NO_x formation moves down, and NO_x is distributed in most areas of the lower part of precalciner. When Y^*_{CRM} is above 1.2, as the location of CRM inlet moves up, the interception effect of CRM stream becomes more obvious. As a result, NO_x generated by the combustion is concentrated at those areas below CRM inlet. For the situation that kiln gas contains NO, the similar phenomenon can be also observed. Within Y= –0.7 m to 0 m, there is an area with low NO_x concentration in spite of a high NO_x concentration at the inlet of kiln gas. With increasing Y^*_{CRM}, this area gradually shrinks in size. Instead, NO_x concentration in the range of –0.7 m to 0 m increases as a whole. Even so, most of nitrogen oxides are still reduced to N_2 in the range of Y= –0.7 m to 1.0 m. This should be attributed to the effects of CRM on the flow field. The addition of CRM at a relatively high position strengthens the mixing process, which is conducive to the reduction of NO_x.

The location of CRM inlet not only affects the formation and reduction of NO_x, but directly influences the decomposition ratio of CRM in the precalciner. In this work, the decomposition ratio of CRM is defined as follows:

$$\gamma = \frac{F_{CaO}\times M_t/56}{M_{CaCO_3}/100}\times 100\% \tag{24}$$

where F_{CaO} is the mass fraction of CaO at the outlet of the precalciner; M_t denotes the total mass flow rate at the outlet of precalciner, kg/s; M_{CaCO_3} represents the feeding rate of $CaCO_3$, kg/s.

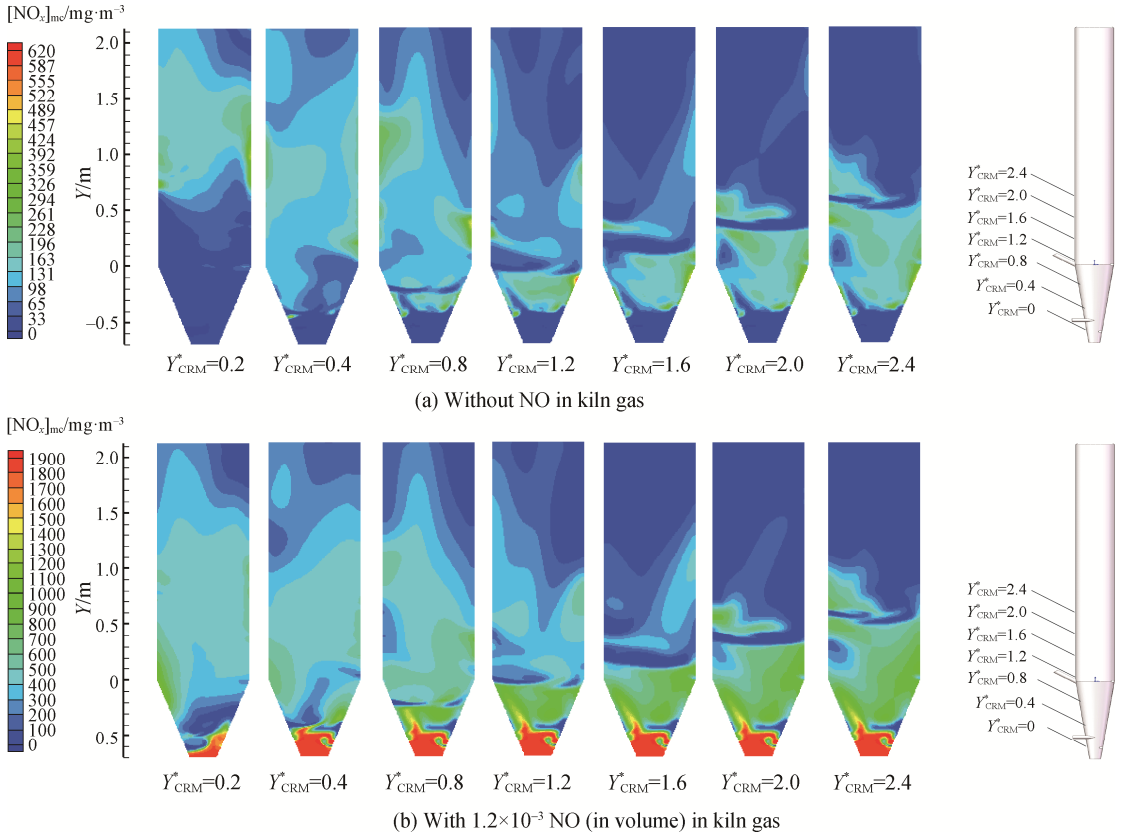

Fig. 15 Mass concentration distribution of NO_x (section Z=0) in the lower part of the precalciner for different Y^*_{CRM}

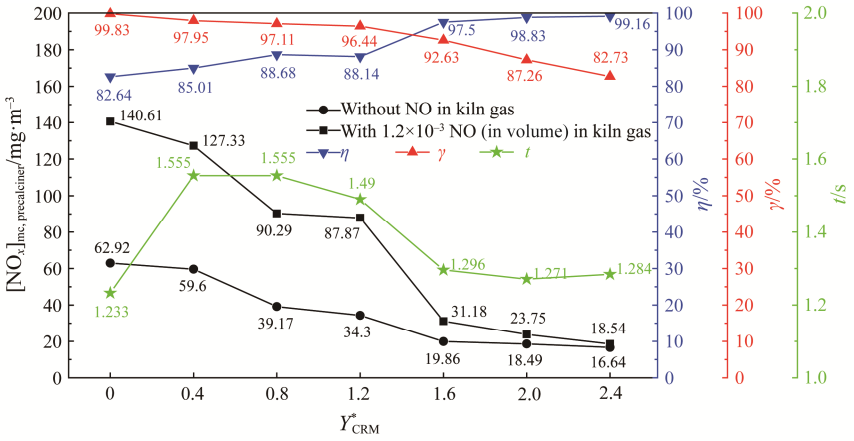

Fig. 16 Effects of Y^*_{CRM} on NO_x emission, reduction rate, decomposition ratio and residence time

Fig. 16 illustrates the effects of Y^*_{CRM} on NO_x emission, reduction rate, decomposition and residence time. With the increase of Y^*_{CRM}, NO_x emission gradually decreases no matter whether kiln gas contains nitric oxide or not. Correspondingly, the reduction rate shows an overall upward trend (The rising speed gradually slows down) while the decomposition rate shows an overall downward trend (The decline speed gradually accelerates). And residence time increases first and then decreases with the increase of Y^*_{CRM}. Nevertheless, Y^*_{CRM}=1.2 seems to be a turning point. The reduction rate at this point (88.14%) slightly decreases in comparison to that at Y^*_{CRM}=0.8 (88.68%), while it sharply rises to 97.5% at Y^*_{CRM}=1.6. The curve of decomposition ratio and residence time also exhibits the similar phenomenon. The decomposition ratio and residence time decreases slowly at Y^*_{CRM}<1.2, and sharply declines when Y^*_{CRM} is more than 1.2. At Y^*_{CRM}=1.6, both reduction rate and decomposition ratio maintain at a high level, i.e., 97.5% and 92.63%. When Y^*_{CRM} rises to 2.4, the decomposition

ratio decreases to 82.73% although the reduction rate increases to 99.16%. In practical engineering, the decomposition ratio of CRM must be more than 90% before entering the rotary kiln for the calcination. Therefore, the trade-off between NO_x removal and decomposition ratio must be considered. From the present simulation results, Y^*_{CRM}=1.6 is the optimum value that can guarantee both reduction rate and decomposition rate.

5. Conclusions

In our previous work, an innovative denitrification method, i.e., fuel in-situ reduction (FISR), was proposed to cut NO_x emission from cement industry [18, 19]. In order to better guide the engineering application, the optimization of FISR method was further investigated by using CFD method in the present work. The pilot-scale precalciner used in the previous experiment was selected as research objection. Based on the verification of the reliability and accuracy of mathematical model, a series of simulations were conducted to deeply explore the effects of various factors on NO_x emission, such as initial NO concentration and oxygen content in kiln gas, location of tertiary air inlet, addition of CRM and feeding location. After adopting FISR method (pretreated fuel, i.e., PF combustion), NO_x emission at the outlet of precalciner drops to 144.66 mg/m^3 from 479.98 mg/m^3 (pulverized coal, i.e., PC combustion) in the case of no further optimization, which proves the effectiveness of FISR method from a numerical point of view. With increasing the initial concentration of NO in kiln gas (from 7×10^{-4} to 12×10^{-4}), NO_x emission increases linearly, but the reduction rate of NO_x changes little and always maintains above 80%. Oxygen content in kiln gas has a significant effect on NO_x emission. Excessive high oxygen concentration in kiln gas will not only promote the conversion of fuel-N in PF to nitrogen oxides, but weaken the reduction of NO_x caused by PF in the precalciner. When oxygen content in kiln gas exceeds 4%, this negative effect becomes more obvious. The staged tertiary air could further help to reduce NO_x emission and the location of first-stage tertiary air (tertiary air-I) was optimized in the present work. The optimal dimensionless location of tertiary air-I is $Y^*_{TA\text{-}I}$=0.6 where NO_x emission can reach 31.19 mg/m^3 corresponding to the highest reduction rate of NO. Because of heat absorption and disturbance effect, the addition of CRM can reduce the formation of NO_x and promote the reduction of NO. On this basis, the feeding location of CRM was further optimized. The simulation results show that Y^*_{CRM}=1.6 is the optimum dimensionless location where both reduction rate of NO and decomposition ratio of CRM can be maintained at a high level.

Acknowledgements

This work is financially supported by "Transformational Technologies for Clean Energy and Demonstration", Strategic Priority Research Program of the Chinese Academy of Sciences (Grant number XDA21040300), and Youth Innovation Promotion Association of the Chinese Academy of Sciences (Grant number Y201642).

Conflict of Interest

REN Qiangqiang is a guest editor for Journal of Thermal Science and was not involved in the editorial review or the decision to publish this article. All authors declare that there are no competing interests.

References

[1] NDRS (National Development and Reform Commission), Operation of building materials industry from January to December 2020. https://www.ndrc.gov.cn/fgsj/tjsj/jjyx/mdyqy/202102/t20210226_1268404.html, 2021 (accessed on March 8, 2021).

[2] Hua S.B., Tian H.Z., Wang K., et al., Atmospheric emission inventory of hazardous air pollutants from China's cement plants: Temporal trends, spatial variation characteristics and scenario projections. Atmospheric Environment, 2016, 128: 1–9.

[3] Fan W.Y., Zhu T.L., Sun Y.F., et al., Effects of gas compositions on NO_x reduction by selective non-catalytic reduction with ammonia in a simulated cement precalciner atmosphere. Chemosphere, 2014, 113: 182–187.

[4] Wang Y.L., Song Y.H., Cui S.P., et al., Study on reduction of nitrogen oxide by pyrolysis pickling sludge. Bulletin of the Chinese Ceramic Society, 2020, 39(8): 2678–2682. (in Chinese)

[5] Li S., Ge Y.F., Wei X.L., Experiment on NO_x reduction by advanced reburning in cement precalciner. Fuel, 2018, 224: 235–240.

[6] Liu R.C., Jiang F.Y., Liu Z.Q., Comments on NO_x emission abatement in cement industry. Advanced Materials Research, 2012, 422: 509–513.

[7] Lv G., Lu J.D., Cai L.Q., et al., Experimental study on the dynamic process of NO reduction in a precalciner. Industrial & Engineering Chemistry Research, 2011, 50 (8): 4366–4372.

[8] Shi C.T., Cai J., Ren Q.Q., et al., Research progress of low NO_x emission control technologies in coal-fired cement kilns. Clean Coal Technology, 2020, 26(1): 174–183. (in Chinese)

[9] Conroy G.H., Low NO_x pyro-systems design and operation. IEEE Transactions on Industry Applications, 1992, 29(5): 303–330.

[10] Du L., Jin B.S., Zheng X., et al., Effect of reburning zone conditions on NO reduction efficiency in an online precalciner-type kiln system. Environmental Progress & Sustainable Energy, 2016, 35(2): 439–446.

[11] Chen D.G., Li Z.S., Cai N.S., Numerical simulation and analysis of reductive atmosphere in air staged pulverized coal combustion. Clean Coal Technology, 2019, 25(1): 109–122. (in Chinese)

[12] Yang X.H., Cai R.X., Zhang Y., et al., Effect of air grading technology on NO_x formation of coal gas combustion in a calciner. Clean Coal Technology, 2019, 25(3): 75–81. (in Chinese)

[13] Fu S.L., Song Q., Tang J.S., et al., Effect of CaO on the selective non-catalytic reduction deNO_x process: Experimental and kinetic study. Chemical Engineering Journal, 2014, 249: 252–259.

[14] Bai B.Y., Qiao Q., Li J.H., et al., Synthesis of three-dimensional ordered mesoporous MnO_2 and its catalytic performance in formaldehyde oxidation. Chinese Journal of Catalysis, 2016, 37(1): 27–31.

[15] Bai B.Y., Qiao Q., Li J.H., et al., Progress in research on catalysts for catalytic oxidation of formaldehyde. Chinese Journal of Catalysis, 2016, 37(1): 102–122.

[16] Gao F.Y., Tang X.L., Yi H.H., et al., Promotional mechanisms of activity and SO_2 tolerance of Co- or Ni-doped MnO_x-CeO_2 catalysts for SCR of NO_x with NH_3 at low temperature. Chemical Engineering Journal, 2017, 317: 20–31.

[17] Yang J., Ren S., Zhang T.S., et al., Iron doped effects on active sites formation over activated carbon supported Mn-Ce oxide catalysts for low-temperature SCR of NO. Chemical Engineering Journal, 2020, 379: 122398.

[18] Wu H.X., Cai J., Ren Q.Q., et al., A thermal and chemical fuel pretreatment process for NO_x reduction from cement kiln. Fuel Processing Technology, 2020, 210: 106556.

[19] Wu H.X., Cai J., Ren Q.Q., et al., An efficient and economic denitration technology based on fuel pretreatment for cement cleaner production. Journal of Cleaner Production, 2020, 272: 122669.

[20] Chen Z.B., Ye F., Gao C., Numerical simulation of NSP cement NO_x formation and control technology. Advanced Materials Research, 2011, 356–360: 1605–1608.

[21] Mikulcic H., Vujanovic M., Duic N., Improving the sustainability of cement production by using numerical simulation of limestone thermal degradation and pulverized coal combustion in a cement calciner. Journal of Cleaner Production, 2015, 88: 262–271.

[22] Nakhaei M., Grévain D., Jensen L.S., et al., NO emission from cement calciners firing coal and petcoke: a CPFD study. Applications in Energy and Combustion Science, 2021, 5: 100023.

[23] Nakhaei M., Wu H., Grévain D., et al., CPFD simulation of petcoke and SRF co-firing in a full-scale cement calciner. Fuel Processing Technology, 2019, 196: 106153.

[24] Sha Y.T., Jin J., Song B., et al., Study on NO_x reduction with syngas reburning. Journal of China Coal Society, 2010, 35(10): 1712–1716.

[25] Chen W.Y., Ma L., Effect of heterogeneous mechanisms during reburning of nitrogen oxide. AIChE Journal, 1996, 42: 1968–1976.

[26] Sørensen C.O., Johnsson J.E., Jensen A.D., Reduction of NO over wheat straw char. Energy and Fuels, 2001, 15(6): 1359–1368.

[27] Stanmore B.R., Tschamber V., Brilhac J.F., Oxidation of carbon by NO_x, with particular reference to NO_2 and N_2O. Fuel, 2008, 87(2): 131–146.

[28] Li X.G., Ma B.G., Hu Z.W., Computational modeling of aerodynamic characteristics in sprayed and spiraled precalciner. Communications in Nonlinear Science and Numerical Simulation, 2008, 13(6): 1205–1211.

[29] Rahmaniane B., Safaei M.R., Kazi S.N., et al., Investigation of pollutant reduction by simulation of turbulent non-premixed pulverized coal combustion. Applied Thermal Engineering, 2014, 73(1): 1222–1235.

[30] Liu Y., Kao H.T., Numerical simulation of urea based SNCR process in a trinal-sprayed precalciner. Journal of Renewable Materials, 2010, 9(2): 269–294.

[31] Pieper C., Wirtz S., Schaefer S., et al., Numerical investigation of the impact of coating layers on RDF combustion and clinker properties in rotary cement kilns. Fuel, 2021, 283: 118951.

[32] Mei S.X., Xie J.J., Chen X.L., et al., Numerical simulation of the complex thermal processes in a vortexing precalciner. Applied Thermal Engineering, 2017, 125: 652–661.

[33] Yang Y., Zhang Y., Li S.J., et al., Numerical simulation of low nitrogen oxides emissions through cement precalciner structure and parameter optimization. Chemosphere, 2020, 258: 127420.

[34] Vascellari M., Cau G., Influence of turbulence-chemical interaction on CFD pulverized coal MILD combustion modeling. Fuel, 2012, 101: 90–101.

[35] Wang F.F., Li P.F., Mi J.C., et al., A refined global reaction mechanism for modeling coal combustion under moderate or intense low-oxygen dilution condition. Energy, 2018, 157: 764–777.

[36] Su S., Xiang J., Sun L.S., et al., Numerical simulation of nitric oxide destruction by gaseous fuel reburning in a single-burner furnace. Proceedings of the Combustion Institute, 2007, 31(2): 2795–2803.

[37] Hanson R.K., Salimian S., Survey of rate constants in H/N/O Systems. W.C. Gardiner, editor, Combustion Chemistry, 1984, pp. 361–421.

[38] DeSoete G.G., Overall reaction rates of NO and N_2 formation form fuel nitrogen. Symposium (International) on Combustion, 1975, 15(1): 1093–1102.

[39] Bowman C.T., Kinetics of pollutant formation and destruction in combustion. Progress in Energy and Combustion Science, 1975, 1(1): 33–45.

[40] Choi C.R., Kim C.N., Numerical investigation on the flow, combustion and NO_x emission characteristics in a 500 MWe tangentially fired pulverized-coal boiler. Fuel, 2009, 88(9): 1720–1731.

[41] Wu H.X., Ren Q.Q., Cai J., et al., Research on the dynamic process of NO heterogeneous and homogeneous reduction with cement raw meal in vertical tubular reactor. Journal of the Energy Institute, 2020, 93(3): 878–888.